PHYSICAL REVIEW D **86,** 042001 (2012)

Strongly magnetized cold degenerate electron gas: Mass-radius relation of the magnetized white dwarf

Upasana Das* and Banibrata Mukhopadhyay†

Department of Physics, Indian Institute of Science, Bangalore 560012, India

(Received 9 December 2011; published 3 August 2012)

We consider a relativistic, degenerate electron gas at zero temperature under the influence of a strong, uniform, static magnetic field, neglecting any form of interactions. Since the density of states for the electrons changes due to the presence of the magnetic field (which gives rise to Landau quantization), the corresponding equation of state also gets modified. In order to investigate the effect of very strong magnetic field, we focus only on systems in which a maximum of either one, two, or three Landau level(s) is/are occupied. This is important since, if a very large number of Landau levels are filled, it implies a very low magnetic field strength which yields back Chandrasekhar's celebrated nonmagnetic results. The maximum number of occupied Landau levels is fixed by the correct choice of two parameters, namely, the magnetic field strength and the maximum Fermi energy of the system. We study the equations of state of these one-level, two-level, and three-level systems and compare them by taking three different maximum Fermi energies. We also find the effect of the strong magnetic field on the mass-radius relation of the underlying star composed of the gas stated above. We obtain an exciting result that it is possible to have an electron-degenerate static star, namely, magnetized white dwarfs, with a mass significantly greater than the Chandrasekhar limit in the range 2.3–2.6$M_\odot$, provided it has an appropriate magnetic field strength and central density. In fact, recent observations of peculiar type Ia supernovae—SN 2006gz, SN 2007if, SN 2009dc, SN 2003fg—seem to suggest super-Chandrasekhar-mass white dwarfs with masses up to 2.4–2.8$M_\odot$ as their most likely progenitors. Interestingly, our results seem to lie within these observational limits.

DOI: 10.1103/PhysRevD.86.042001 PACS numbers: 67.85.Lm, 51.30.+i, 71.70.Di, 97.20.Rp

I. INTRODUCTION

Neutron stars are known to have high magnetic fields as large as 10^{12} G or more on their surfaces. Several magnetic white dwarfs have also been discovered with surface fields from about 10^5 G to 10^9 G [1–6], and the physics of these objects have also been studied from a long time [7–9]. It is likely that stronger fields exist in the centers of neutron stars or even white dwarfs, the limit to which is set by the scalar virial theorem [10]:

$$2T + W + 3\Pi + \tilde{M} = 0, \tag{1}$$

where T is the total kinetic (rotational) energy, W the gravitational potential energy, Π arises due to the internal energy, and $\tilde{M}$ the magnetic energy. Since T and Π are both positive, the maximum magnetic energy can be compared to, but can never exceed, the gravitational energy in an equilibrium configuration. For a star of mass M and radius R, this gives $(4\pi R^3/3)(B_{\rm max}^2/8\pi) \sim GM^2/R$, or $B_{\rm max} \sim 2 \times 10^8 (M/M_\odot)(R/R_\odot)^{-2}$ G. For white dwarfs, this limit is 10^{12} G. Ostriker and Hartwick [11] had constructed models of magnetic white dwarfs with magnetic field strength $B \sim 10^{12}$ G at the center but with a much smaller field at the surface. Thus, high interior magnetic fields in white dwarfs, although rarely observed in nature so far, are not completely implausible.

It was proposed by Ginzburg [12] and Woltjer [13] that the magnetic flux $\phi_B \sim 4\pi BR^2$ of a star is conserved during its evolution and subsequent collapse to form a remnant degenerate star (flux freezing phenomenon). Thus, degenerate stars of small size and large magnetic fields are expected to be formed from parent stars which originally could have quite high magnetic fields of the order $\sim 10^8$ G [14,15]. Thus, the study of such highly magnetized degenerate stars will help us understand the origin and evolution of stellar magnetic fields.

The mass-radius relation for (nonmagnetic) white dwarfs was first determined by Chandrasekhar [16]. He obtained a maximum mass for stable white dwarfs, known as the famous Chandrasekhar limit ($\sim 1.44M_\odot$), such that electron degeneracy pressure is just adequate to counteract gravitational collapse of the star. Suh *et al.* [17] obtained the mass-radius relation for white dwarfs with $B \sim 4.4 \times 10^{11-13}$ G. They, however, worked in the weak field limit (thus ignoring Landau quantization) and applied Euler-MacLaurin expansion to the equation of state of a fully degenerate electron gas in a strong magnetic field [10], in order to recover the usual equation of state in the absence of a magnetic field. They found that both the mass and radius of magnetic white dwarfs increase compared to nonmagnetic white dwarfs, having the same central density.

*upasana@physics.iisc.ernet.in
†bm@physics.iisc.ernet.in

In this paper, we consider a relativistic, degenerate electron gas at zero temperature under the influence of a strong, uniform, static magnetic field. We neglect any form of interactions between the electrons. We study the effect of a strong magnetic field on the equation of state of the degenerate matter and consequently obtain the mass-radius relation for a collapsed static star which might be composed of such matter. In order to highlight the effect of Landau quantization of electrons due to a strong magnetic field, we restrict our systems to have, at most, one, two, or three Landau level(s).

We hypothesize the possibility of the existence of purely electron-degenerate stars with extremely high magnetic fields $\sim 10^{15}$–10^{17} G at the center, plausibly strongly magnetized white dwarfs. We also investigate the possibility of such stars having a mass greater than the Chandrasekhar limit, in the range 2.3–2.6$M_\odot$. In a simple analytical framework, existence of such stars has already been reported recently [18], and its astrophysical implications based on numerical analysis was also discussed [19]. Interestingly, recent observations of peculiar type 1a supernovae—SN 2006gz, SN 2007if, SN 2009dc, SN 2003fg—seem to suggest super-Chandrasekhar-mass white dwarfs as their most likely progenitors [20,21]. These white dwarfs are believed to have masses up to 2.4–2.8$M_\odot$. A proposed mechanism by which these white dwarfs exceed the Chandrasekhar limit is mass accretion from a binary companion accompanied by differential rotation [22]. This is fundamentally different from what we are proposing here. However, these observations are quite stimulating as, not only do they support the existence of super-Chandrasekhar mass white dwarfs, but also our results seem to lie within the observational limits.

The paper is organized as follows. In the next section, we first recall how the equation of state of a cold electron-degenerate gas gets modified due to the presence of a strong magnetic field and then state the numerical procedure followed to obtain results. Subsequently, in Sec. III, we discuss the numerical results describing the nature of the equations of state and the mass-radius relations. In Sec. IV, we elaborate on some of the key points of this work, for example, the timescale of magnetic field decay, comparison with Chandrasekhar's standard results, unstable branch of the mass-radius relations, the justifications for a constant magnetic field, the nonrelativistic equation for hydrostatic equilibrium, neglecting Coulomb interactions, and the anisotropy in pressure due to a strong magnetic field. Finally, in Sec. V, we summarize our findings with conclusions.

II. EQUATION OF STATE FOR A FREE ELECTRON GAS IN A STRONG MAGNETIC FIELD

A. Basic equations

The energy states of a free electron in a uniform magnetic field are quantized into what is known as Landau orbitals, which define the motion of the electron in a plane perpendicular to the magnetic field. On solving the Schrödinger equation in an external, uniform, and static magnetic field directed along the z axis, one obtains the following dispersion relation [23]:

$$E_{\nu,p_z} = \nu\hbar\omega_c + \frac{p_z^2}{2m_e}, \tag{2}$$

where quantum number ν denotes the Landau level and is given by

$$\nu = j + \frac{1}{2} + \sigma, \tag{3}$$

with j being the principal quantum number of the Landau level ($j = 0, 1, 2, \ldots$), $\sigma = \pm\frac{1}{2}$, the spin of the electron, m_e the rest mass of the electron, $\hbar$ the Planck constant, and p_z the momentum of the electron along the z axis which may be treated as continuous (the motion along the field is not quantized).

The cyclotron energy is $\hbar\omega_c = \hbar(eB/m_ec)$, where e is the charge of the electron, c the speed of light, and B the magnetic field.

Now, the electrons can become relativistic in either of the two cases:

(i) when the density is high enough such that the mean Fermi energy of an electron exceeds its rest-mass energy,

(ii) when the cyclotron energy of the electron exceeds its rest-mass energy.

We can define a critical magnetic field strength B_c from the relation $\hbar\omega_c = m_ec^2$, which gives $B_c = m_e^2c^3/\hbar e = 4.414 \times 10^{13}$ G. Thus, in order to study the effect of a strong magnetic field ($B \gtrsim B_c$) on the equation of state of a relativistic, degenerate electron gas, we have to solve the relativistic Dirac equation. We mention here that, for the present purpose, the magnetic field considered in the electron-degenerate star originates due to the flux freezing phenomenon during the gravitational collapse of the parent star. The energy eigenstates in this case turn out to be [10]

$$E_{\nu,p_z} = \left[p_z^2c^2 + m_e^2c^4\left(1 + \nu\frac{2B}{B_c}\right)\right]^{1/2}. \tag{4}$$

The main effect of the magnetic field is to modify the available density of states for the electrons. The number of states per unit volume in an interval Δp_z for a given Landau level ν is $g_\nu(eB/h^2c)\Delta p_z$, where g_ν is the degeneracy which arises due to the Landau level splitting, such that $g_\nu = 1$ for $\nu = 0$ and $g_\nu = 2$ for $\nu \geq 1$. Therefore, the electron-state density in the absence of a magnetic field

$$\frac{2}{h^3}\int d^3p, \tag{5}$$

has to be replaced with

$$\sum_{\nu} \frac{2eB}{h^2 c} g_\nu \int dp_z \tag{6}$$

in the case of a nonzero magnetic field.

Now, in order to calculate the electron number density n_e at zero temperature, we have to evaluate the integral in Eq. (6) from $p_z = 0$ to $p_F(\nu)$, which is the Fermi momentum of the electron for the Landau level ν, to obtain [10]

$$n_e = \sum_{\nu=0}^{\nu_m} \frac{2eB}{h^2 c} g_\nu p_F(\nu). \tag{7}$$

The Fermi energy E_F of the electrons for the Landau level ν is given by

$$E_F^2 = p_F(\nu)^2 c^2 + m_e^2 c^4 \left(1 + 2\nu \frac{B}{B_c}\right). \tag{8}$$

The upper limit ν_m of the summation in Eq. (7) is derived from the condition that $p_F(\nu)^2 \geq 0$, which implies $E_F^2 \geq m_E^2 c^4 (1 + 2\nu \frac{B}{B_c})$, and we obtain

$$\nu \leq \frac{\epsilon_F^2 - 1}{2B_D} \tag{9}$$

or

$$\nu_m = \frac{\epsilon_{F\max}^2 - 1}{2B_D}, \tag{10}$$

where $\epsilon_F = E_F/m_e c^2$ is the dimensionless Fermi energy, $B_D = B/B_c$ the dimensionless magnetic field, and $\epsilon_{F\max} = E_{F\max}/m_e c^2$ the dimensionless maximum Fermi energy of a system for a given B_D and ν_m. We note that ν_m is taken be the nearest lowest integer in Eq. (10). For example, if $0 \leq \nu_m < 1$ for a particular value of $\epsilon_{F\max}$ and B_D, then the upper limit is taken to be $\nu_m = 0$.

If we define a dimensionless Fermi momentum $x_F(\nu) = p_F(\nu)/m_e c$, then Eqs. (7) and (8) may be written as

$$n_e = \frac{2B_D}{(2\pi)^2 \lambda_e^3} \sum_{\nu=0}^{\nu_m} g_\nu x_F(\nu) \tag{11}$$

and

$$\epsilon_F = [x_F(\nu)^2 + 1 + 2\nu B_D]^{1/2} \tag{12}$$

or

$$x_F(\nu) = [\epsilon_F^2 - (1 + 2\nu B_D)]^{1/2}, \tag{13}$$

where $\lambda_e = \hbar/m_e c$ is the Compton wavelength of the electron. The matter density ρ can be written as

$$\rho = \mu_e m_H n_e, \tag{14}$$

where μ_e is the mean molecular weight per electrons and m_H the mass of the hydrogen atom.

The electron energy density at zero temperature is

$$\begin{aligned}\varepsilon_e &= \frac{2B_D}{(2\pi)^2 \lambda_e^3} \sum_{\nu=0}^{\nu_m} g_\nu \int_0^{x_F(\nu)} E_{\nu,p_z} d\left(\frac{p_z}{m_e c}\right) \\ &= \frac{2B_D}{(2\pi)^2 \lambda_e^3} m_e c^2 \sum_{\nu=0}^{\nu_m} g_\nu (1 + 2\nu B_D) \psi\left(\frac{x_F(\nu)}{(1 + 2\nu B_D)^{1/2}}\right),\end{aligned} \tag{15}$$

where

$$\psi(z) = \int_0^z (1 + y^2)^{1/2} dy = \frac{1}{2} z\sqrt{1 + z^2} + \frac{1}{2} \ln(z + \sqrt{1 + z^2}). \tag{16}$$

Then, the pressure of an electron gas in a magnetic field is given by

$$\begin{aligned}P_e &= n_e^2 \frac{d}{dn_e}\left(\frac{\varepsilon_e}{n_e}\right) = -\varepsilon_e + n_e E_F \\ &= \frac{2B_D}{(2\pi)^2 \lambda_e^3} m_e c^2 \sum_{\nu=0}^{\nu_m} g_\nu (1 + 2\nu B_D) \eta\left(\frac{x_F(\nu)}{(1 + 2\nu B_D)^{1/2}}\right),\end{aligned} \tag{17}$$

where

$$\eta(z) = \frac{1}{2} z\sqrt{1 + z^2} - \frac{1}{2} \ln(z + \sqrt{1 + z^2}). \tag{18}$$

B. Procedure

Referring to the qualitative discussion by Lai and Shapiro [10], let ν_m also denote the maximum number of Landau levels occupied by a cold gas of electrons in a magnetic field. In this case, from Eq. (10), ν_m will be the nearest highest integer. Then, if $\nu_m \gg 1$, the Landau energy level spacing becomes a very small fraction of the Fermi energy, and the discrete sum over ν can be replaced by an integral, and we get back the nonmagnetic results. From Eq. (10), we see that if the magnetic field strength is high (for a fixed Fermi energy), i.e., $B_D \gg 1$, then ν_m is small, and the electrons are restricted to the lower Landau levels only. It is in this case that the magnetic field plays an important role in influencing the equation of state for the relativistic degenerate gas.

Since we are investigating the effects of a high magnetic field in this work, we fix ν_m such that it can only take values 1, 2, or 3, which we call a one-level, two-level, and three-level system, respectively. To clarify further, by one-level system, we mean where only the ground Landau level, $\nu = 0$, is occupied; two-level means where both the ground and the first ($\nu = 1$) Landau levels are occupied; and three-level means where the ground, first, and second ($\nu = 2$) Landau levels are occupied. Now, from Eq. (10), we see that once we fix ν_m, we obtain a fixed B_D on supplying a desired $E_{F\max}$, which corresponds to the maximum possible density (in a star which corresponds to

TABLE I. Parameters for the equations of state in Fig. 1.

$E_{F\max}$	Maximum Landau level(s) $\nu_{\rm m}$	B_D	B in units of 10^{15} G
$2m_ec^2$	1	1.5	0.066
	2	0.75	0.033
	3	0.5	0.022
$20m_ec^2$	1	199.5	8.81
	2	99.75	4.40
	3	66.5	2.94
$200m_ec^2$	1	19999.5	882.78
	2	9999.75	441.38
	3	6666.5	294.26

its central density) for that ν_m. Hence, in our framework, the magnetic field is in accordance with the density of the system. We choose $E_{F\max} = 2m_ec^2$, $20m_ec^2$ and $200m_ec^2$, and for each, we study the one-level, two-level, and three-level systems, giving a total of 9 cases which are listed in Table I. We mention here that for a given value of $E_{F\max}$, the value of B_D listed here corresponds to a lower limit. For example, when $E_{F\max} = 20m_ec^2$, B_D with a value of 199.5 just results in a one-level system but, if we choose any $B_D > 199.5$, that would also lead to a one-level system.

For each of these cases, we obtain the equation of state by simultaneously solving Eqs. (11), (14), and (17) numerically from $E_F = m_ec^2$ to $E_F = E_{F\max}$, when each value of E_F gives one point in the $P_e - \rho$ plot. In this work, we choose $\mu_e = 2$ throughout. Figure 1 shows the equations of state for the different cases given in Table I, which will be discussed in Sec. III.

If we are to construct the model of a strongly magnetized star made out of electron-degenerate matter, which is approximated to be spherical in the presence of a constant magnetic field, we require solving the following differential equation, which basically comes from the condition of hydrostatic equilibrium [24]:

$$\frac{1}{r^2}\frac{d}{dr}\left(\frac{r^2}{\rho}\frac{dP}{dr}\right) = -4\pi G\rho, \tag{19}$$

where we consider $P = P_e$ throughout this work. See, however, the appendix in order to understand the effect of deviation from spherical symmetry due to the anisotropic effects of a magnetic field, as discussed in Sec. IV G. Since the pressure cannot be expressed as an analytical function of density, unlike that of Chandrasekhar's work [16], we fit the equation of state with the following polytropic relation:

$$P = K\rho^{\Gamma}, \tag{20}$$

with different values of the adiabatic index Γ in different density ranges (K being a dimensional constant). Thus, the actual equation of state is reconstructed using multiple polytropic equations of state. One such fit is shown in Fig. 1(d),

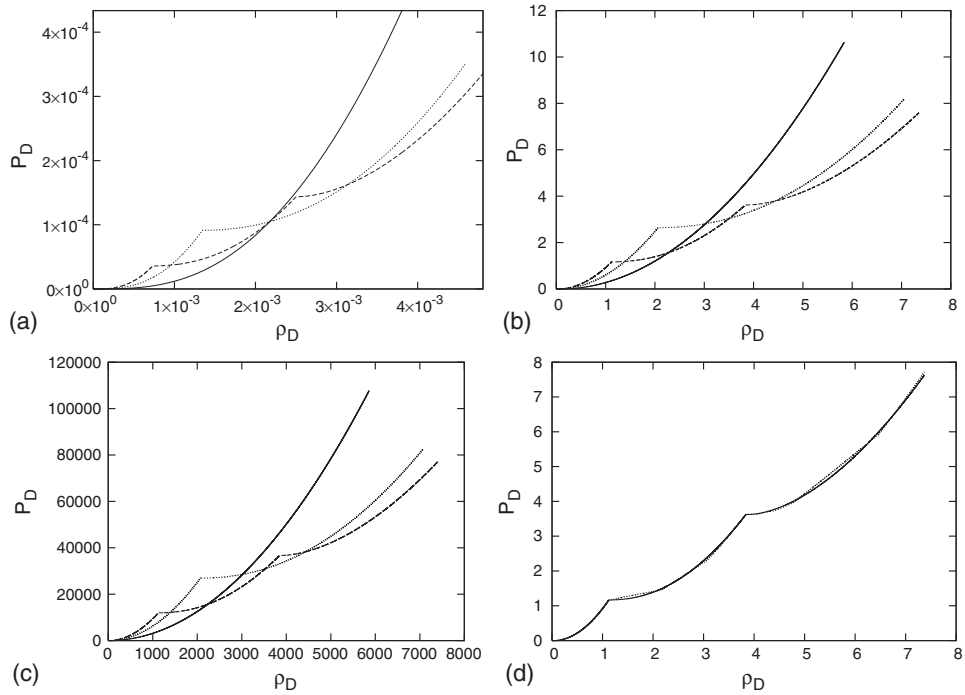

FIG. 1. Equations of state in a strong magnetic field (given in Table I) for (a) $E_{F\max} = 2m_ec^2$, (b) $E_{F\max} = 20m_ec^2$, (c) $E_{F\max} = 200m_ec^2$. In all three cases, the solid line, the dotted line, and the dashed lines indicate one-level, two-level, and three-level systems, respectively. In (d), the solid line is same as the dashed line in (b), but fitted with the dotted line by analytical formalism (see text for details). Here, P_D is the pressure in units of 2.668×10^{27} erg/cc, and ρ_D is the density in units of 2×10^9 gm/cc.

TABLE II. Parameters for the fitting function of the equation of state shown in Fig. 1(d) and the corresponding mass-radius relation shown in Fig. 2(c).

ρ_D in units of 2×10^9 gm/cc	Γ	$n = \frac{1}{\Gamma - 1}$	K in CGS units	$R \propto M^{(1-n)/(3-n)}$
0–0.096	2.9	0.526	4.055	$R \propto M^{0.192}$
0.096–0.307	2.4	0.714	1.284	$R \propto M^{0.125}$
0.307–1.128	2.1	0.909	0.914	$R \propto M^{0.044}$
1.128–2.117	0.35	−1.538	1.105	Unstable
2.117–2.956	4/3	3	0.522	$M \propto R^0$
2.956–3.842	2.0	1.0	0.246	$R \propto M^0$
3.842–4.651	0.35	−1.538	2.225	Unstable
4.651–6.116	4/3	3	0.496	$M \propto R^0$
6.116–7.37	2.0	1.0	0.142	$R \propto M^0$

and the parameters K and Γ are stated in Table II. The motivation behind doing such a fit is the following. First of all, with this fitting, we can determine the effect of a magnetic field on the adiabatic index of the matter. More importantly, once we use an equation of state of the form (20), the problem essentially reduces to solving the Lane-Emden equation which arises in the nonmagnetic case, except that in our case, K and Γ also carry information about the magnetic field in the system.

We briefly recall here the Lane-Emden equation, since we will be referring to some of its solutions in the next section. We start with Eqs. (19) and (20) and write $\Gamma = 1 + \frac{1}{n}$, where n is the polytropic index. Next, two variable transformations are made as follows [24]:

$$\rho = \rho_c \theta^n, \tag{21}$$

where ρ_c is the central density of the star and θ is a dimensionless variable and

$$r = a\xi, \tag{22}$$

where ξ is another dimensionless variable and a is defined as

$$a = \left[\frac{(n+1)K\rho_c^{(1-n)/n}}{4\pi G}\right]^{1/2}, \tag{23}$$

which has the dimension of length. Thus using Eqs. (20)–(23), Eq. (19) reduces to the famous Lane-Emden equation,

$$\frac{1}{\xi^2}\frac{d}{d\xi}\left(\xi^2 \frac{d\theta}{d\xi}\right) = -\theta^n, \tag{24}$$

which can be solved for a given n, subjected to the following two boundary conditions:

$$\theta(\xi = 0) = 1 \tag{25}$$

and

$$\left(\frac{d\theta}{d\xi}\right)_{\xi=0} = 0. \tag{26}$$

If $n < 5$, then θ falls to zero for a finite value of ξ, called ξ_1, which basically denotes the surface of the star where the pressure goes to zero (and then density becomes zero, too, in the present context). The physical radius of the star is then given by

$$R = a\xi_1. \tag{27}$$

We note that the value of n must be such that $n \geq -1$, so that a is real in Eq. (23) and $R \geq 0$ in Eq. (27). Each value of central density ρ_c corresponds to a particular value of radius R and mass M of a star. Substituting a from Eq. (23) in Eq. (27), we find

$$R \propto \rho_c^{(1-n)/2n} = \rho_c^{(\Gamma-2)/2}. \tag{28}$$

The mass of the spherical star (see, however, the appendix discussing the equations for an oblate spheroid) is obtained by integrating the following equation:

$$\frac{dM}{dr} = 4\pi r^2 \rho. \tag{29}$$

Hence,

$$M = 4\pi \int_0^R r^2 \rho dr = 4\pi a^3 \rho_c \int_0^{\xi_1} \xi^2 \theta^n d\xi. \tag{30}$$

Again substituting a from Eq. (23) in Eq. (30), we find

$$M \propto \rho_c^{(3-n)/2n} = \rho_c^{(3\Gamma-4)/2}, \tag{31}$$

and then combining Eqs. (28) and (31), we obtain the following mass-radius relation:

$$R \propto M^{(1-n)/(3-n)} = M^{(\Gamma-2)/(3\Gamma-4)}. \tag{32}$$

In the present work, we do not make the transformations (21) and (22), but directly solve Eq. (19) (in different density regions corresponding to the particular values of Γ or n) subjected to the same boundary conditions as in Eqs. (25) and (26), which are written as

$$\rho(r = 0) = \rho_c \tag{33}$$

and

$$\left(\frac{d\rho}{dr}\right)_{r=0} = 0. \tag{34}$$

Hence, the results in Eqs. (28), (31), and (32) still remain applicable to our case. A plot of R as a function of M gives the mass-radius relation for the magnetic, degenerate static star.

Figure 2 shows the mass-radius relations for the one-level, two-level, and three-level systems with $E_{F\max} = 20m_ec^2$ (results for $E_{F\max} = 2m_ec^2$ and $200m_ec^2$ also show the same trend). Figure 3 shows a comparison between the mass-radius relations for all the cases stated in Table I. All these are discussed in detail in the next section.

III. NUMERICAL RESULTS

A. Equations of state

Now, we come to the discussions of the results obtained. We start with the equations of state shown in Fig. 1. Let us consider the panel (b) which shows the cases with $E_{F\max} = 20m_ec^2$. From Table I, we see that the one-level system (the solid line) for $E_{F\max} = 20m_ec^2$ corresponds to a magnetic field strength $B_D = 199.5$, and the two-level and three level systems (the dotted and dashed lines, respectively) correspond to $B_D = 99.75$ and 66.5, respectively. We notice that the solid curve is free of any kink, the dotted curve has one kink, and the dashed curve has two kinks. The kinks appear when there is a transition from a lower Landau level to the next, and they demarcate regions of the equation of state where the pressure becomes briefly independent of density. Let us consider the two-level systems. The portion of the equation of state below the kink represents the ground Landau level, and the one above the kink represents the first Landau level. As the Fermi energy of the electrons increases, more and more electrons occupy the ground Landau level, and both the density and pressure of the system keep increasing. Once the ground level is completely filled, one observes that, on increasing the Fermi energy of the electrons, the density increases, but the pressure remains fairly constant for a while, after which the pressure again starts increasing with density. It is as if the increase in Fermi energy during the transition is being used by the system to move to a higher Landau level instead of increasing the pressure. This situation seems analogous to that of phase transition in matter (where the temperature remains constant with respect to the input heat energy during the change of phase). Similar features are also seen in Figs. 1(a) and 1(c) for $E_{F\max} = 2m_ec^2$ and $200m_ec^2$, respectively.

Thus, looking at Fig. 1, we observe that in the one-level systems (solid lines), all the electrons are in the ground Landau level, and hence there is no kink. In the two-level systems (dotted lines), as the electrons start filling up the first Landau level, a kink develops in the equation of state. Finally, in the three-level systems (dashed lines), there are two kinks—the one at the lower density indicating transition to the first Landau level and another at the higher density indicating transition to the second Landau level. The value of $E_{F\max}$ determines the maximum density of the system, and hence the positions of the kinks shift accordingly in Figs. 1(a)–1(c).

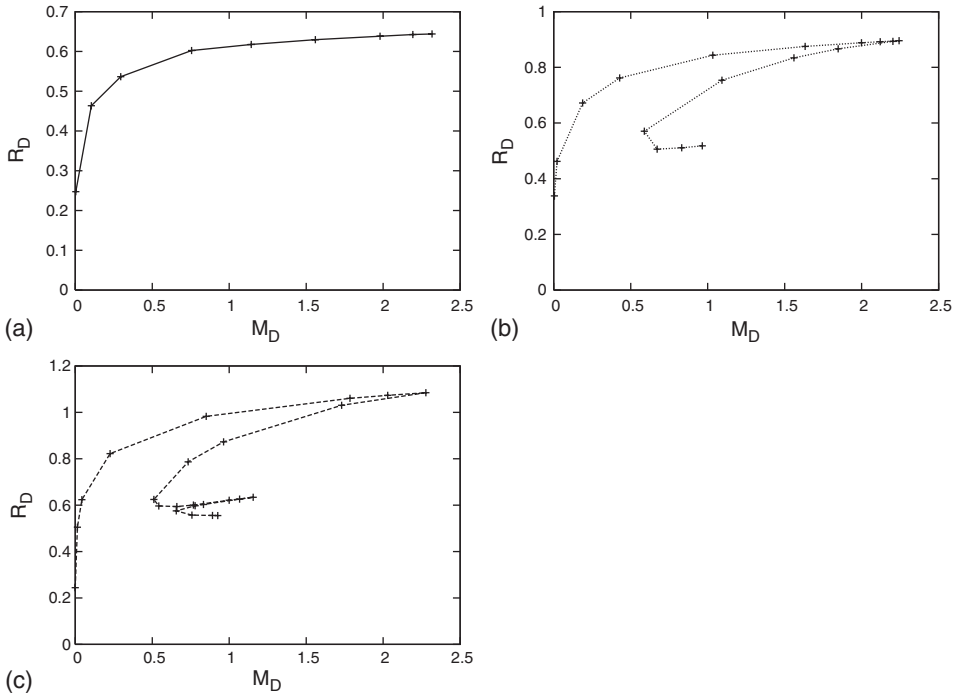

FIG. 2. Mass-radius relations with $E_{F\max} = 20m_ec^2$ for (a) one-level system, (b) two-level system, (c) three-level system. Here, M_D is the mass of the star in units of $M_\odot$, and R_D is the radius of the star in units of 10^8 cm (the solid, dotted, and dashed lines have the same meaning as in Fig. 1).

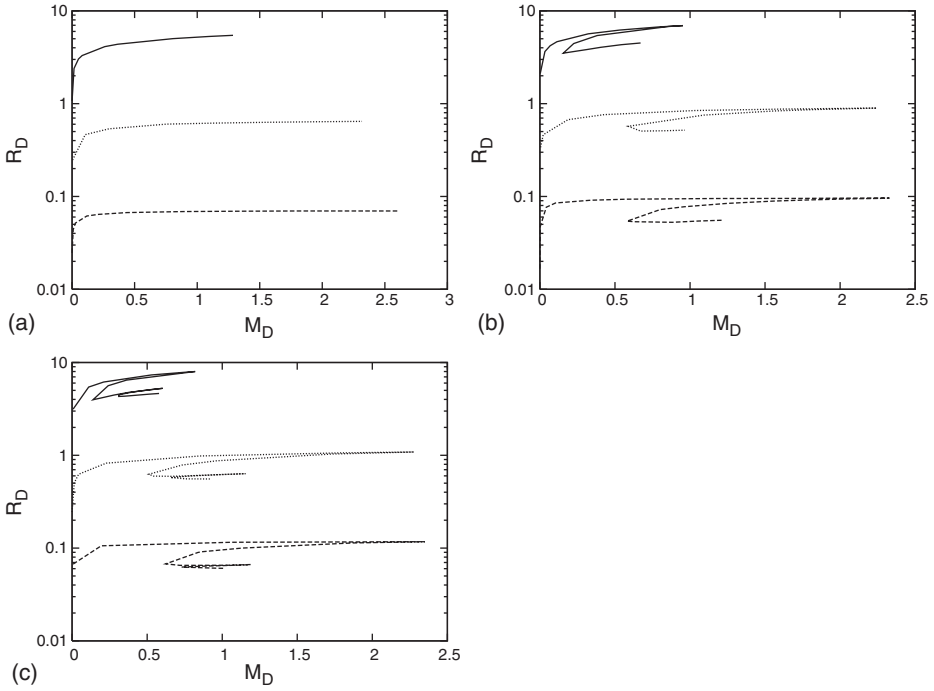

FIG. 3. Comparison of the mass-radius relations, for (a) one-level system, (b) two-level system, (c) three-level system, when the solid, dotted, and dashed lines represent $E_{F\max} = 2m_ec^2$, $20m_ec^2$ and $200m_ec^2$, respectively. In each of the three panels, the y axis is in log scale. See Table I for details.

B. Mass-radius relations

Next, we come to Fig. 2. Here, we show the mass-radius relations for the one-level, two-level, and three level systems with $E_{F\max} = 20m_ec^2$ (the explanation which follows also holds true for the cases with $E_{F\max} = 2m_ec^2$ and $200m_ec^2$). Each point in the mass-radius curve corresponds to a star with a particular value of central density ρ_c which is supplied by us as a boundary condition (R_D and M_D are the dimensionless radius and mass of a star, respectively, as defined in Fig. 2's caption).

Figure 2(a) shows the mass-radius relation for the one-level system ($B_D = 199.5$). We see that, initially, as ρ_c increases, both the mass and radius increase, and then at higher central densities, the radius becomes nearly independent of the mass (we will be explaining later in this section why such a trend is observed). We note that the last point on this curve has a mass $\sim 2.3M_\odot$ and radius $\sim 6.4 \times 10^7$ cm, which corresponds to the maximum density point of the solid curve in Fig. 1(b). This denotes the density ($\sim 1.16 \times 10^{10}$ gm/cc) at which the ground Landau level is completely filled. Thus, a star with this ρ_c and a magnetic field strength of $B = 199.5B_c = 8.81 \times 10^{15}$ G has a mass greater than the Chandrasekhar limit ($\sim 1.44M_\odot$ for $\mu_e = 2$).

Figure 2(b) shows the mass-radius relation for the two-level system ($B_D = 99.75$). In this case, a maximum mass $\sim 2.3M_\odot$ is reached at a radius $\sim 8.9 \times 10^7$ cm for $\rho_c \sim 4.0 \times 10^9$gm/cc, in the same way as in Fig. 2(a) when the ground Landau level is completely filled. After this, there is a turning point in the curve, from where the mass starts decreasing. This turning point corresponds to the kink in the corresponding equation of state [dotted curve in Fig. 1(b)]. During the transition (when 4.0×10^9 gm/cc $< \rho_c \lesssim 8.0 \times 10^9$ gm/cc) from ground to the first Landau level, the radius and mass both decrease with increasing ρ_c. Then, there is a brief range of densities (8.0×10^9 gm/cc $< \rho_c \lesssim 1.2 \times 10^{10}$ gm/cc) where the radius decreases as the mass remains fairly constant, and ultimately at very high densities (1.2×10^9 gm/cc $< \rho_c \lesssim 1.5 \times 10^{10}$ gm/cc), the radius is again nearly independent of the mass, as in the uppermost branch.

Figure 2(c) shows the mass-radius relation for the three-level system ($B_D = 66.5$). Here, we see two turning points, denoted by the decrease of both mass and radius, which correspond to the two kinks in the corresponding equation of state [dashed curve in Fig. 1(b)]. The maximum mass at the first turning point $\sim 2.3M_\odot$ is reached at a radius $\sim 1.1 \times 10^8$ cm for $\rho_c \sim 2.2 \times 10^9$ gm/cc (the first kink in the equation of state). The mass at the second turning point is $\sim 1.2M_\odot$ which has a radius $\sim 6.3 \times 10^7$ cm for $\rho_c \sim 7.6 \times 10^9$ gm/cc (the second kink in the equation of state). Just after either of the turning points denoted by the decrease of radius and mass both, briefly, the radius decreases as the mass remains almost constant, and, finally, the radius becomes nearly independent of mass. The maximum mass $\sim 2.3M_\odot$ occurs at the central density where the ground Landau level is completely filled and transition to the first Landau level is about to start. We observe that this density

follows $\rho_c(\text{three-level}) < \rho_c(\text{two-level}) < \rho_c(\text{one-level})$ as is also seen from the positions of the kinks in Fig. 1.

In order to explain this behavior in further detail, we resort to the Lane-Emden relations (28), (31), and (32). From Eq. (28), we note that if $\Gamma > 2$, then R increases with ρ_c, and if $\Gamma = 2$, then R is independent of ρ_c. From Eq. (31), we note that if $\Gamma > 4/3$, then M increases with ρ_c, and if $\Gamma = 4/3$, then M is independent of ρ_c. Finally from Eq. (32), we note that if $\Gamma > 2$, then R increases with M, if $\Gamma = 2$, then R is independent of M, and if $\Gamma = 4/3$, then M is independent of R. This is exactly what is observed in Fig. 2.

Let us look again at the mass-radius relation corresponding to Fig. 2(c) (also see Table II). At very low densities, Γ is ~ 3 (which is the case for nonrelativistic electrons in the ground Landau level; $P_e(= P) \propto \rho^3$; see Ref. [25]), and the value of Γ keeps decreasing with increasing density. Up to the first turning point density $\rho_c \sim 2.2 \times 10^9$ gm/cc, both the radius and mass keep increasing with ρ_c, and then the radius becomes nearly independent of mass when $\Gamma \sim 2$. Then, Γ suddenly drops to the small value ~ 0.35 which marks the onset of the transition from the ground Landau level to the first Landau level. In this region, the pressure becomes independent of density, revealing an unstable zone in the equation of state (see detailed discussion in Sec. IV E). As the density increases further, Γ approaches the relativistic value of $4/3$. In this regime, we see that the radius decreases slightly as the mass does not change significantly, as is also true for the mass-radius relation in the classical nonmagnetic case for $\Gamma = 4/3$ [see Fig. 4(b)]. Next, Γ takes up a value of 2, and the radius again becomes nearly independent of mass until it reaches the second turning point at density $\rho_c \sim 7.6 \times 10^9$ gm/cc. Again, during the transition from the first Landau level to the second, Γ drops to 0.35, followed by values of $4/3$ and 2, which have the same explanations as stated above.

We also observe that, for a certain range of masses in the two-level and three-level systems, it is possible to have multiple values of the radius for a given value of mass. For instance, looking at the two-level system in Fig. 2(b) in the range ~ 0.6–$1.0 M_\odot$, we observe that the same value of mass corresponds to three different values of the radius. Let us call them R_1, R_2, and R_3, such that $R_1 > R_2 > R_3$ and $\rho_c(R_1) < \rho_c(R_2) < \rho_c(R_3)$. To explain why we observe such a behavior, we recall that B_D of the system is such that ν_m is fixed for a given value of $E_{F\max}$ (see Table I for the values). In Fig. 2(b), $B_D = 99.75$ ensures that the system can have, at the most, two Landau levels (ground and first), but to what extent they will be filled depends on the Fermi energy of the electrons ($\leq E_{F\max}$). For low central densities (i.e., low Fermi energy), the electrons occupy only the ground Landau level. In order for the electrons to start occupying the first Landau level, the central density of the star must be adequately high. Thus, based on previous discussion for the mass-radius curves in

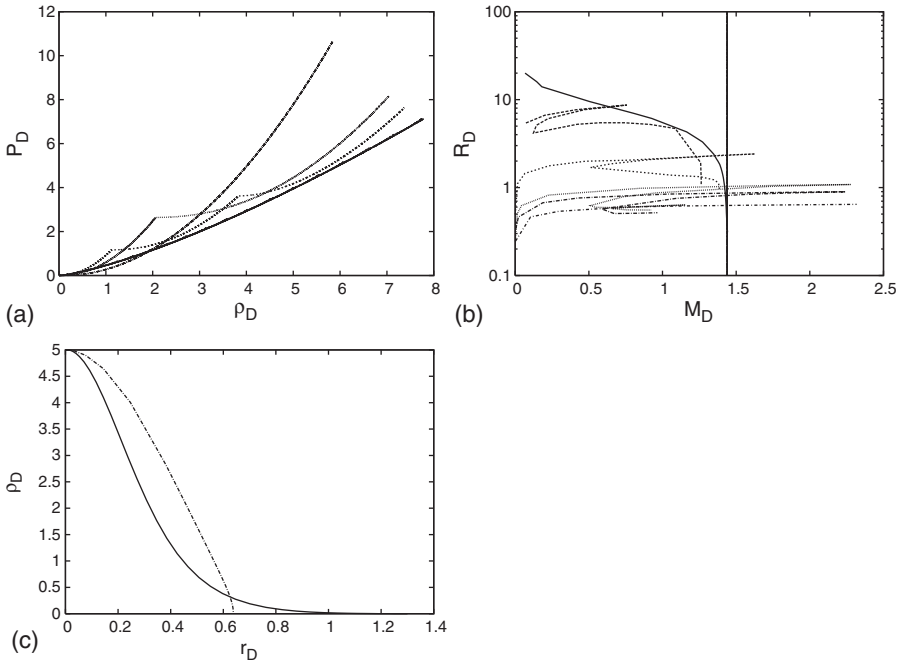

FIG. 4. Comparison with Chandrasekhar's nonmagnetic results for $E_{F\max} = 20 m_e c^2$. (a) Equations of state—the solid line represents Chandrasekhar's equation of state. The dotted-dashed, dotted, and dashed lines represent the one-level ($\nu_m = 1$), two-level ($\nu_m = 2$), and three-level ($\nu_m = 3$) systems, respectively. The equation of state for $\nu_m = 20$ is also shown, which appears as a series of kinks on top of the solid line. (b) Mass-radius relations—the vertical line marks the $1.44 M_\odot$ limit, and the solid line represents Chandrasekhar's mass-radius relation. From top to bottom, the other lines represent the cases for $\nu_m = 500$, 20, 3, 2, and 1, respectively (the y axis is in log scale). (c) Density as a function of radius inside a nonmagnetized star (solid line) and a star having $\nu_m = 1$ (dotted-dashed line), both having the same central density $\rho_c = 5$ in units of 2×10^9 gm/cc.

Fig. 2, it is possible that the same mass of a star corresponds to more than one radius, depending on the Landau level occupancy. Now, R_1 lies on the branch of the mass-radius relation which corresponds to the stars in which the electrons occupy only the ground Landau level, while R_3 lies on the branch which corresponds to the electrons occupying the first Landau level (the ground level being already filled). R_2 lies on the unstable branch of the mass-radius relation (see discussion in Sec. IV E) when the electrons are in the transition mode form the ground to the first Landau level. The three-level system in Fig. 2(c) can also be explained likewise, except that it has two additional possible radii corresponding to the same mass due to the presence of the second Landau level. In the one-level system in Fig. 2(a), multiple values of radius are not observed because the magnetic field ($B_D = 199.5$) is such that the electrons can occupy only the ground Landau level.

Finally, we come to Fig. 3. For each of the Figs. 3(a), 3(b) and 3(c), the value of $E_{F\max}$ increases from the top to the bottom curve, and we see that the overall radius decreases from the top to the bottom curve. We also note that an increase in $E_{F\max}$ corresponds to an increase in the magnetic field for a fixed ν_m, which means that as the magnetic field strength increases, the degenerate stars become more and more compact in size. The same trend has been observed in the case of neutron stars with a high magnetic field [26–28] (see discussion in Sec. IV B.) Interestingly, as seen from Fig. 3(a), for $E_{F\max} = 200m_ec^2$, the maximum mass of the star is even higher than that of $E_{F\max} = 20m_ec^2$, which is $\sim 2.6M_\odot$. Also to be noted is the fact that for a given ν_m, the curve corresponding to $E_{F\max} = 20m_ec^2$ covers almost the same range in mass as that of the $E_{F\max} = 200m_ec^2$ curve, while the curve for $E_{F\max} = 2m_ec^2$ covers a considerably smaller range in mass. The reason behind this saturation at higher $E_{F\max}$ may be due to the fact that a Fermi energy $\sim 2m_ec^2$ corresponds to very low density such that the electrons are, at the most, only mildly relativistic. By the time Fermi energy reaches a value of about $20m_ec^2$ (which corresponds to high density), the electrons have become highly relativistic, giving rise to denser, more massive stars, and, hence, further increase of $E_{F\max}$ could not bring any new effect in the system.

IV. DISCUSSIONS

A. Time scale of decay of magnetic field

Generally, the magnetic fields inside an electron-degenerate star undergo Ohmic decay. The time scale for this is given by $t_{\rm ohm} = \frac{4\pi\sigma_E L^2}{c^2}$, where σ_E is the electrical conductivity and L is the length scale over which the magnetic field changes. Theoretical calculations of Ohmic decay in isolated, cooling white dwarfs, which are generally known in nature, show that the magnetic field changes little over their lifetime [29–31]. Cumming [32] estimated a lowest-order decay time as

$$t_{\rm ohm} \approx 10^{10}\ {\rm yrs}\left(\frac{\rho_c}{3\times 10^6\ {\rm gm/cc}}\right)^{1/3}\left(\frac{\rm R}{10^9\ {\rm cm}}\right)^{1/2}\left(\frac{10\langle\rho\rangle}{\rho_c}\right), \tag{35}$$

where $\langle\rho\rangle$ is the mean density of the star. For the three stars represented in Fig. 5(d), the above time scale turns out to

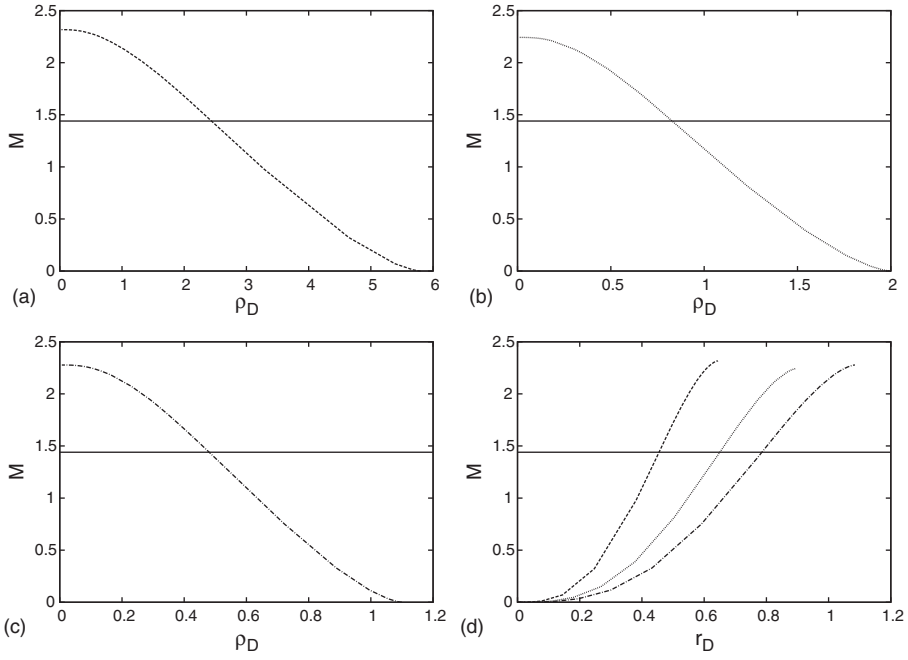

FIG. 5. Mass as a function of density within an electron-degenerate star with B_D (a) 199.5 (dashed line), (b) 99.75 (dotted line), (c) 66.5 (dotted-dashed line), for $E_{F\max} = 20m_ec^2$. (d) Variation of mass as a function of radius within the stars in (a), (b), and (c). The horizontal line indicates the $1.44M_\odot$ limit. The radius r_D is in units of 10^8 cm. See Table I for details.

be $\gtrsim 10^9$ years. Thus, we can say that the magnetic fields of these stars do not decay significantly via Ohmic dissipation in their lifetime. However, while for $B \lesssim 10^{11}$ G, Ohmic decay is the dominant phenomenon, for $B \sim 10^{12} - 10^{13}$ G, decay is supposed to take place via Hall drift, and for $B \gtrsim 10^{14}$ G, it undergoes ambipolar diffusion [33]. Note that all the decay time scales stated above are valid only for normal or nonsuperfluid matter. Hence, while they might be unrealistic for neutron stars [34], these time scales are applicable to white dwarfs since they do not have a superconducting core [35,36].

Heyl and Kulkarni [33] examined the consequences of the magnetic field decay in magnetars having surface field 10^{14} G to 10^{16} G by using an appropriate cooling model and by solving the following decay equation:

$$\frac{dB}{dt} = -B\left(\frac{1}{t_{\text{ohmic}}} + \frac{1}{t_{\text{ambip}}} + \frac{1}{t_{\text{Hall}}}\right). \tag{36}$$

The strongly magnetized white dwarfs considered in the present work have central magnetic field strengths $\sim 10^{15}$ G, which is comparable to the surface field strengths of magnetars. It is then likely that the magnetic fields in both these cases would undergo similar decay mechanisms. The decay of such strong fields is dominated by ambipolar diffusion [33]. However, for a typical initial field strength of 10^{15} G, the magnetic field remains nearly constant up to about 10^5 years, and in the next 100 years, its value decreases by, at most, an order of magnitude [33]. As discussed in Sec. IV C below, it is the central magnetic field which is crucial for the super-Chandrasekhar mass of the white dwarfs. Thus, applying the above results to these magnetized white dwarfs, we can conclude that the central field will not decay appreciably for a long period of time.

An alternate scenario could arise if the magnetized white dwarfs are accreting. In this case, the heat generated due to accretion decreases the electrical conductivity of the surface of the star, causing a faster decay of the (surface) magnetic field due to a reduced Ohmic decay time scale. However, as the mass of the star increases, it becomes more compact, and the current carrying accreted material is pushed deeper into the star. Since conductivity is a steeply increasing function of density, the higher conductivity of the denser inner region of the star will again slow down further decay of the magnetic field [37].

Since we are working with magnetic field strengths $B > B_c$, one might be concerned about the process of electron-positron pair creation (via Schwinger process) at the expense of magnetic energy, which might lead to a reduction of the field strength. However, Canuto and Chiu [38–40] and also Daugherty *et al.* [41] showed that it is impossible to have spontaneous pair creation in a magnetic field alone, irrespective of its strength. Now, from Maxwell's equations in a steady state, we have

$$\nabla \times \mathbf{B} = \frac{4\pi}{c}\mathbf{j}, \tag{37}$$

and Ohm's law states

$$\mathbf{E} = \frac{\mathbf{j}}{\sigma_E}, \tag{38}$$

when $\mathbf{E}$ is the electric field and $\mathbf{j}$ the current density. Thus, for an electric field to be generated, the magnetic field must vary with space as seen from Eq. (37). However, in this work, we have chosen a constant magnetic field, which leads to $\mathbf{j} = 0$ and hence $\mathbf{E} = 0$ from Eq. (38). Now, the main effect of the magnetic field, which is to give rise to a mass exceeding the Chandrasekhar limit, is restricted to the high-density region, where the field remains essentially constant. Thus, our choice of a constant magnetic field is justified (see Sec. IV C for detailed discussion). Moreover, since the magnetic field in the degenerate star is generated due to the flux freezing phenomenon, it incorporates the fact that the conductivity σ_E is very large. Thus, even if the magnetic field is highly inhomogeneous, from Eq. (38), we see that the electric field generated would again be negligible. Thus, the electron-degenerate stars in this work are magnetically dominated systems, i.e., both the magnetic field strength is very high ($B > B_c$) and the electric field strength is negligible. Recently, Jones [42] calculated the cross section for photon-induced pair creation in very high magnetic fields and has arrived at the result that there is a rapid decrease of the pair creation cross section at $B > B_c$. Hence, one can ignore the effect of pair creation in reducing the magnetic field strength in these stars.

B. Comparison with Chandrasekhar's results

In Fig. 4, we put together our results along with Chandrasekhar's result for nonmagnetic white dwarfs to obtain a more complete picture. Figure 4(a) shows the equation of state obtained by Chandrasekhar and those corresponding to the one- ($\nu_m = 1$), two- ($\nu_m = 2$), and three-level ($\nu_m = 3$) systems [same as in Fig. 1(b)]. Interestingly, the equation of state for $\nu_m = 20$ almost grazes Chandrasekhar's equation of state, except for the appearance of a series of kinks. This clearly shows that, as the magnetic field strength decreases, or, equivalently, as the maximum number of occupied Landau levels increases, the equation of state approaches Chandrasekhar's equation of state.

Figure 4(b) represents the mass-radius relations corresponding to the equations of state shown in Fig. 4(a). The mass-radius relation for $\nu_m = 500$ (500 Landau levels) is also shown. We observe that, as the magnetic field strength decreases or as the maximum number of occupied Landau levels increases, the mass-radius relation approaches the nonmagnetic relation, and one recovers Chandrasekhar's mass limit.

Figure 4(b) also shows that the stars of a given mass become more and more compact in size as the magnetic field strength increases. In order to explain this behavior, we resort to Figs. 4(a) and 4(c). Let us, for simplicity, look at Chandrasekhar's equation of state (solid line) and that of the one-level system (dotted-dashed line), which

corresponds to $B = 199.5B_c$, in Fig. 4(a). We notice that at low densities, the dotted-dashed line lies below the solid line, and at higher densities, $\rho_D \gtrsim 2$, the dotted-dashed line lies above the solid line. In other words, the equation of state for the one-level system is softer than Chandrasekhar's equation of state at low densities, which means that the pressure does not rise with density as rapidly as that in Chandrasekhar's case. This trend reverses at higher densities, and the equation of state for the one-level case becomes stiffer than that of Chandrasekhar's. Now, matter with a softer equation of state is less efficient in counteracting gravity, and hence stars made out of such matter will be more compact in size. Keeping this in mind, we now look at Fig. 4(c). Figure 4(c) shows the variation of density with radius, within a nonmagnetized star and a magnetized star with $\nu_m = 1$ (one-level), both having the same central density ($\rho_c = 5$). We mention here that for ease of explanation, we have chosen a high central density such that the equations of state for both the stars cover almost the entire range of density. We observe that for a given radius, density for the magnetized star is higher than that of the nonmagnetized star for a large range, from $\rho_D = \rho_c = 5$ to $\rho_D \sim 0.3$. But at very low densities, $\rho_D < 0.3$, the density of the magnetized star sharply falls to zero due to smaller pressure, leading to a smaller star ($R = 6.4 \times 10^7$ cm) than in the nonmagnetized case ($R = 1.3 \times 10^8$ cm). From the analysis of the equations of state for these two stars, we can say that if the equation of state of the magnetized star would have remained stiffer than the nonmagnetized star throughout, then the magnetized star would have a larger radius, as, in this case, the pressure would be more efficient in counteracting the gravitational collapse of the star. But this is not true. At very low densities, the equation of state suddenly becomes softer for the magnetized star, and the pressure is not able to counteract gravity efficiently, causing the star to collapse rapidly. Hence, the density goes to zero very rapidly, causing the star to have a (much) smaller radius.

We also note from Fig. 4(b) that as the magnetic field strength increases, the probability that the stars will have masses exceeding the Chandrasekhar limit increases. From Fig. 4(c), we see that the density of the magnetized star is much higher than that of the nonmagnetized star, except for a very small range of low densities. Thus, calculating the total mass of the stars from Eq. (29), we obtain a much higher value for the magnetized star.

C. Choice of constant magnetic field

Figures 5(a)–5(c) show the variation of mass as a function of density within a magnetized electron-degenerate star for three different magnetic field strengths. In all the cases, we note that, by the time the density falls to about half the value of the central density, the mass has increased significantly, crossing the Chandrasekhar limit (indicated by the horizontal line) soon after. Hence, although we have considered a constant magnetic field, the effect of the magnetic field is restricted to the high-density regime, where the field remains essentially constant in reality. Hence, we can also interpret this constant magnetic field as the central magnetic field of the star. This would be more clear from the description of the variation of magnetic field given by Refs. [26,43], which show that an inhomogeneous magnetic profile in a compact star could be such that the magnetic field is nearly constant throughout most of the star and then gradually falls off close to the surface (see Fig. 5b in Ref. [26]). Thus, choosing an inhomogeneous magnetic profile would not affect our main finding that the Chandrasekhar mass limit can be exceeded for high magnetic field strengths.

D. Choice of nonrelativistic equation of hydrostatic equilibrium

Figure 5(d) shows the variation of mass as a function of radius within the stars represented in Figs. 5(a)–5(c). All these stars have a total mass $\sim 2.3 M_\odot$, and hence their Schwarzschild radius $R_g = \frac{2GM}{c^2} = 6.8 \times 10^5$ cm. Now, general relativistic effects usually start becoming important at a radius $\lesssim 10R_g$, i.e., $r_D \lesssim 0.068$ for the above-mentioned stars. However, from Fig. 5(d), we see that for all the three stars, the contribution to the mass from a radius $<10R_g$, i.e., the central region, is negligible. Contribution to the mass rather effectively starts from a radius $r_D \gtrsim 0.13$ ($\sim 20R_g$), and the Chandrasekhar limit is crossed at $R_g \sim 66$, 95, and 118, for the stars represented by the dashed, dotted, and dotted-dashed lines, respectively. Thus, significant contribution to the total mass of the stars comes from a region well beyond the regime of general relativity. Hence, one need not consider the Tolman-Oppenheimer-Volkoff equation, and our choice of the nonrelativistic equation of equilibrium, Eq. (19), is justified.

E. Unstable branch of the mass-radius relations

Figure 6(a) shows the variation of density as a function of radius inside the degenerate stars having $E_{F\,\max} = 20 m_e c^2$ and $B = 99.75 B_c$. If we look at the equation of state for the two-level system with $E_{F\,\max} = 20 m_e c^2$, i.e., the dotted line in Fig. 1(b), we see that both $\rho_D = 1.5$ and 2 lie below the density at which transition takes place from the ground Landau level to the first Landau level. For stars with these central densities, the pressure rises monotonically with density throughout, and one forms a stable star. From the corresponding curves (solid and dashed) in Fig. 6(b), also we note that the sound speed (c_s) varies smoothly with radius, reaching a maximum value at the center. Both the mass and radius of these stars increase with central density, and, hence, they lie on the uppermost branch of the mass-radius relation in Fig. 2(b).

Now, $\rho_D = 2.5$ lies on the plateau following the kink in the equation of state. A star having this central density will have within it a zone where pressure does not steadily

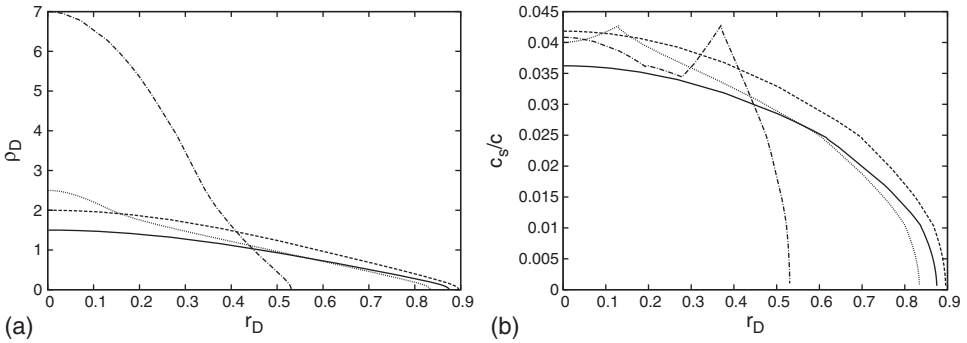

FIG. 6. (a) Density and (b) sound speed in units of c, as a function of radius, inside the stars having $E_{F\max} = 20m_ec^2$ and $B = 99.75B_c$. The solid, dashed, dotted, and dotted-dashed lines represent the stars with central densities 1.5, 2, 2.5, and 7, in units of 2×10^9 gm/cc, respectively.

increase with density, but is nearly constant. Thus, such a star will tend to collapse faster under gravity and hence will have a smaller radius. From the dotted line in Fig. 6(a), we see that the density of such a star falls steeply to zero compared to the $\rho_D = 2$ case, indicated by the dashed line. The corresponding curve in Fig. 6(b) shows a peak in c_s at the radius where pressure starts becoming independent of density. Since mass of the star is calculated using Eq. (29), such a star has a smaller mass too due to smaller size. These stars lie on the middle branch of the corresponding mass-radius relation. Since these stars consist of an unstable zone mentioned above, we argue that they constitute the somewhat unstable branch in the mass-radius relation.

Finally, let us choose a larger density, say $\rho_D = 7$, which lies on that portion of the equation of state above the kink, where pressure again rises monotonically with density, but not as steeply as that in the regions around $\rho_D = 1.5$ and 2. Although these stars also have an unstable zone inside them, but softer pressure in a large range of density, which together cause them to have a smaller radius, their central density is very high. As a result, their mass starts increasing again, as can be inferred from the dotted-dashed line in Fig. 6(a). The c_s again shows a sharp peak indicating the appearance of an unstable zone within the star. These stars constitute the bottommost branch of the mass-radius relation.

F. Neglecting Coulomb interactions

The distance between nuclei in highly magnetized electron-degenerate stars could be as small as 50 Fermi. The Coulomb repulsion energy between electrons $\frac{e^2}{r}$, at the separation of 50 Fermi, is of the order of 4×10^{-8} ergs, which is quite less than the rest-mass energy of an electron $m_ec^2 \sim 8 \times 10^{-7}$ ergs. There can be Coulomb interaction between electrons and the ions, which is given by $\frac{Ze^2}{r}$. Commonly, electron-degenerate stars consist of helium, carbon, oxygen, etc., so that Z can have a value of 10 at the most. Hence, the Coulomb interaction energy would still be less than or, at most, the same order as the rest-mass energy. Thus, we can neglect the effects of Coulomb interaction for the present purpose.

G. Anisotropy in pressure due to a strong magnetic field

The strong magnetic field causes the pressure to become anisotropic [27,44,45]. The total energy momentum tensor due to both matter and magnetic field is to be given by

$$T^{\mu\nu} = T^{\mu\nu}_m + T^{\mu\nu}_f, \tag{39}$$

where

$$T^{\mu\nu}_m = \epsilon_m u^\mu u^\nu - P_m(g^{\mu\nu} - u^\mu u^\nu) \tag{40}$$

and

$$T^{\mu\nu}_f = \frac{B^2}{4\pi}\left(u^\mu u^\nu - \frac{1}{2}g^{\mu\nu}\right) - \frac{B^\mu B^\nu}{4\pi}, \tag{41}$$

when $\epsilon_m = \epsilon_e$ is the matter energy density given by Eq. (15) and $P_m = P_e$ is the matter pressure given by Eq. (17). The first term in Eq. (41) is equivalent to magnetic pressure, while the second term gives rise to the magnetic tension. If B is along the z axis, then we have

$$T^{\mu\nu}_f = \begin{bmatrix} \frac{B^2}{8\pi} & 0 & 0 & 0 \\ 0 & \frac{B^2}{8\pi} & 0 & 0 \\ 0 & 0 & \frac{B^2}{8\pi} & 0 \\ 0 & 0 & 0 & -\frac{B^2}{8\pi} \end{bmatrix}. \tag{42}$$

Thus, we see that pressure becomes anisotropic. The total pressure in the perpendicular direction to the magnetic field is given by

$$P_\perp = P_m + \frac{B^2}{8\pi}, \tag{43}$$

and the parallel direction to the magnetic field is given by

$$P_\parallel = P_m - \frac{B^2}{8\pi}. \tag{44}$$

Now, the parallel pressure becomes negative if the magnetic pressure exceeds the fluid pressure. In order to

understand this effect, we write the component of $T_f^{\mu\nu}$ along the z axis as

$$T_f^{zz} = \frac{B^2}{8\pi} - \frac{B^2}{4\pi}. \tag{45}$$

The second term $-B^2/4\pi$ corresponds to an excess negative pressure or tension along the direction to the magnetic field. Thus, the total energy momentum tensor can be written as

$$T^{\mu\nu} = \begin{bmatrix} \epsilon_m + \frac{B^2}{8\pi} & 0 & 0 & 0 \\ 0 & P_m + \frac{B^2}{8\pi} & 0 & 0 \\ 0 & 0 & P_m + \frac{B^2}{8\pi} & 0 \\ 0 & 0 & 0 & \left(P_m + \frac{B^2}{8\pi}\right) - \frac{B^2}{4\pi} \end{bmatrix}. \tag{46}$$

The strong magnetic field also reveals anisotropy due to magnetization pressure [27]. Hence, actually, the pressure in the perpendicular direction to the magnetic field is given by

$$P_\perp = P_m + \frac{B^2}{8\pi} - \mathcal{M}\mathcal{B}, \tag{47}$$

where $\mathcal{M}$ is the magnetization of the system, which is given by

$$\mathcal{M} = -\frac{\partial \epsilon_m}{\partial B}. \tag{48}$$

However, for the magnetic fields considered in the present work exhibiting super-Chandrasekhar masses, $B^2/8\pi \gg \mathcal{M}\mathcal{B}$. Therefore, we do not include the magnetization term in the pressure which does not affect the result practically for the present purpose.

Here, we refer to the work by Bocquet *et al.* [46], which models rotating neutron stars with magnetic fields, by using an extension of the electromagnetic code used by Bonazzola *et al.* [47]. They observed that the component of the total energy momentum tensor along the symmetry axis becomes negative (equivalent to $T^{zz} < 0$ in our case), since the fluid pressure decreases more rapidly than the magnetic pressure away from the center of the star. This happens because the combined fluid-magnetic medium develops a tension. As a result of this magnetic tension, the star displays a pinch across the symmetry axis and assumes a flattened shape. A similar effect is expected to occur in our work, where the magnetic tension will be responsible for deforming the magnetized white dwarf along the direction to the magnetic field, and turns it into a kind of oblate spheroid. Hence, one should be cautious before considering Eq. (19), which is applicable for a spherical star [45].

However, in this work, we consider a constant magnetic field, since our interest is to see the effect of the magnetic field of the central region of the white dwarf, where the field is supposed to be (almost) constant (see Sec. IV C). Thus, even if we use either the parallel or the perpendicular pressure in the hydrostatic equilibrium equation (19), B does not appear explicitly in the equation ($dB/dr = 0$)—only the gravitational field will be modified due to deformation. Hence, it is still possible to have super-Chandrasekhar-mass white dwarfs—only they will be deformed in shape due to the strong field, which might even render a more massive white dwarf (as is discussed in the appendix).

V. SUMMARY AND CONCLUSIONS

We have studied the effect of a high magnetic field on the equation of state of purely electron-degenerate matter at zero temperature. In the equation of state, we have considered only the electron degeneracy pressure modified by the strong magnetic field. We have focused on those Landau-quantized systems in which the maximum number of Landau level(s) occupied is one, two, or three, which we have named to be one-level, two-level, and three-level system, respectively.

We have found that whenever a lower Landau level is completely filled and the next higher level is to be filled, a kink appears in the equation of state, followed by a plateau—which is a small region where the pressure becomes nearly independent of the density. The one-level system, which has only the ground Landau level filled, has no kink; the two-level system has one kink at the ground-to-first-level transition; and the three-level system has two kinks, one at the ground-to-first and the other at the first-to-second-level transition. We have studied each of these systems at three maximum Fermi energies $E_{F\,\mathrm{max}} = 2m_ec^2$, $20m_ec^2$ and $200m_ec^2$ and obtained the mass-radius relations of the corresponding stars.

The mass-radius relations show one or more turning points, denoted by the decrease of both mass and radius, which corresponds to the kink(s) in the equation of state. The most interesting result obtained is that there are possible stars found on the mass-radius relations whose mass exceeds the Chandrasekhar limit. They could be potential magnetized white dwarfs. The maximum mass obtained is about 2.3–2.6$M_\odot$ and is seen to occur for various combinations of central density, magnetic field strength, and the maximum number of occupied Landau levels. Interestingly, such supermassive white dwarfs have been suggested to be the most likely progenitors of recently observed type Ia supernovae [20,21]. Out of the equations of state considered in the present work, the system with the lowest magnetic field which gives rise to this mass is the three-level system with $E_{F\,\mathrm{max}} = 20m_ec^2$, $B_D = 66.5$ (or $B = 2.94 \times 10^{15}$ G), and the corresponding central density is 2.2×10^9 gm/cc.

The nature of the mass-radius relations is governed by whether the system is one-level, two-level, or three-level

and is independent of the value of $E_{F\max}$. However, $E_{F\max}$ determines how relativistic the system is. For instance, the Chandrasekhar mass limit is not exceeded for a low $E_{F\max}$ (say $= 2m_e c^2$), no matter what the central density is. We have, however, observed that as $E_{F\max}$ increases, which corresponds to an increase in the magnetic field strength, the degenerate stars become more compact in size.

As discussed, the minimum magnetic field required to have a $2.3M_\odot$ degenerate star is $B = 2.94 \times 10^{15}$ G. The magnetic field of the original star of radius $R_\odot$, which collapses into the above degenerate star of radius $\sim 10^8$ cm, turns out to be $\sim 6 \times 10^9$ G, based on the flux freezing theorem. Existence of such stars is not ruled out [15]. However, the anisotropy in pressure due to strong magnetic field causes a deformation in the white dwarfs which adopt a flattened shape. This effect of flattening leads to more massive white dwarfs, even at relatively lower magnetic-field strengths.

One might wonder why highly magnetized white dwarfs have not yet been observed. A plausible reason could be that the surface magnetic field is being screened due to some physical processes. For instance, if the white dwarf is in a binary system and is accreting matter from its companion, as is proposed for type Ia supernovae progenitors, then the plasma which is being deposited on the surface of the star could induce an opposite magnetic moment. This would result in a reduction of the surface field strength. However, the central magnetic field strength, which is presumably unaffected by the above processes, could be several orders of magnitude higher than the surface field. Indeed as seen in Sec. IV C, it is the central field which is crucial for exceeding the Chandrasekhar mass limit.

ACKNOWLEDGMENTS

This work was partly supported by the ISRO grant ISRO/RES/2/367/10-11. We would like to thank the anonymous referees, D. Bhattacharya and E. J. Ferrer for their useful comments, which helped us greatly in improving this work.

APPENDIX

In order to estimate the effect of deviation from spherical symmetry due to the magnetic field, we have performed a few calculations. If the magnetic field is very strong, then the magnetic tension will flatten the star along the direction to the field (as discussed in Sec. IV G). If we consider the white dwarf to be an oblate spheroid with the z axis being the symmetry axis, then its equation is given by

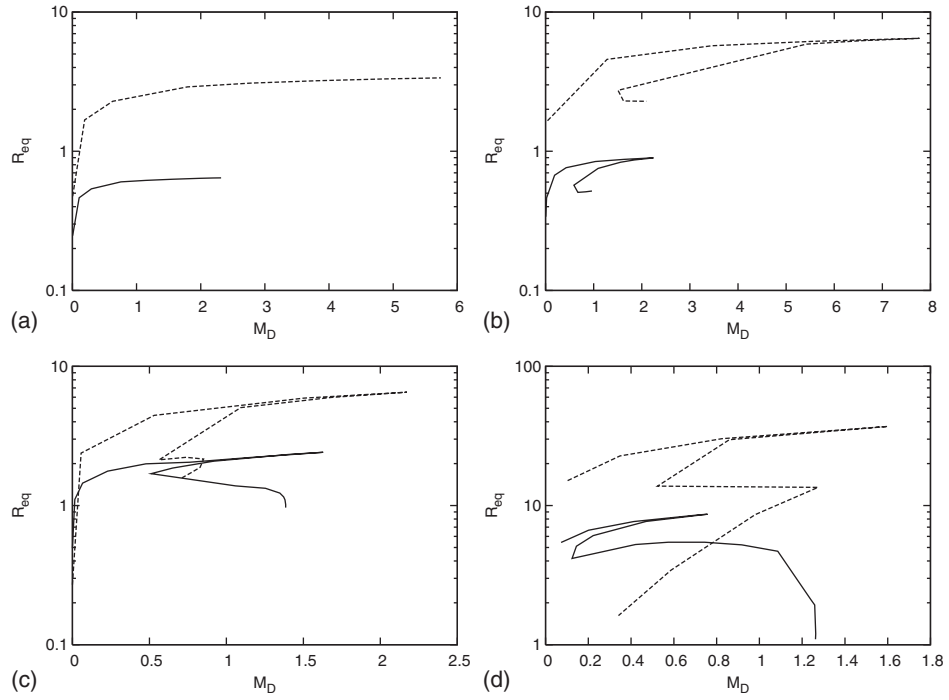

FIG. 7. Mass-radius relations with $E_{F\max} = 20m_e c^2$ for (a) one-level system ($\nu_m = 1$), (b) two-level system ($\nu_m = 2$), (c) 20-level system ($\nu_m = 20$), and (d) five hundred-level system ($\nu_m = 500$). Here, M_D is the mass of the white dwarf in units of $M_\odot$, and $R_{\rm eq}$ is the equatorial radius of the white dwarf in units of 10^8 cm. All the solid lines represent the mass-radius relations for the cases, if the stars would have been spherical. The dashed lines in (a) and (b) represent the mass-radius relations for highly flattened (strongly magnetized) white dwarfs, while the dashed lines in (c) and (d) represent the mass-radius relations for less flattened (relatively weakly magnetized) white dwarfs. In all the four panels, the y axis is in log scale.

$$\frac{r_{\rm eq}^2}{a^2} + \frac{z^2}{c^2} = 1, \tag{A1}$$

where $r_{\rm eq}^2 = x^2 + y^2$, the semi-axis a is the equatorial radius of the spheroid, and c is the distance from the center to the pole along the symmetry axis ($c < a$ for an oblate spheroid).

The equatorial force balance equation can be written as

$$\frac{1}{\rho}\frac{dP}{dr_{\rm eq}} = -\frac{GM}{r^2}\left(\frac{r_{\rm eq}}{r}\right), \tag{A2}$$

where $r^2 = r_{\rm eq}^2 + z^2$. The above equation for hydrostatic equilibrium has to be supplemented by an equation to determine the mass of the star. Now,

$$dM = \rho dV \tag{A3}$$

and the volume element for an oblate spheroid is given by

$$dV = \pi r_{\rm eq}(z)^2 dz. \tag{A4}$$

For a simpler visualization, one can also assume a cylindrical geometry, and the equation for the mass can be given by

$$\frac{dM}{dr_{\rm eq}} = 2\pi r_{\rm eq} h \rho, \tag{A5}$$

where h denotes an average height of the cylinder (assuming that the density does not change appreciably with z) and is a parameter which quantifies the degree of flattening. At high field strengths, the white dwarf will be more flattened, and h will be small. At low field strengths, it is likely that the star will be less flattened, and h will have a larger value. Keeping this in mind, we solved the above equations and obtained the mass-radius relations for some of the cases as shown in Fig. 7.

The one-level and two-level systems have strong magnetic fields, and the corresponding mass-radius relations for the spherical case are denoted by the solid lines in Figs. 7(a) and 7(b). From the dashed lines in Figs. 7(a) and 7(b), we see that the flattened white dwarfs could have much higher masses than the perfectly spherical ones. Interestingly, we note from the dashed lines of Figs. 7(c) and 7(d) that, even for much lower magnetic field strengths ($B = 4.4 \times 10^{14}$ G for $\nu_m = 20$ and 1.8×10^{13} G for $\nu_m = 500$), the Chandrasekhar-mass limit is exceeded even if one includes the corresponding reduced flattening effect—these white dwarfs were sub-Chandrasekhar for the spherical cases. One can also see that the radius of the stars represented by the dashed lines is larger than that represented by the solid lines. One must note here that for the dashed lines, this radius is the equatorial radius, which will automatically be larger than the spherical radius as a consequence of the flattening effect.

Hence, the effect of flattening leads to a more massive star. The effect is very similar to the flattening due to centrifugal force in rapidly rotating stars, which are known to be more massive than their slow-rotating counterparts (e.g., Ref. [46]). These are also shown to have larger mass in the presence of a high magnetic field. Thus, the strong magnetic field is responsible for increasing the mass of the white dwarfs, while the deformation (or flattening) of the white dwarf due to the field further adds on to the mass. Therefore, our estimate of the mass of the white dwarf, in fact, just sets a lower bound. More interestingly, flattening effects due to magnetic field will render super-Chandrasekhar white dwarfs even at a smaller magnetic field—such relatively low magnetized white dwarfs are more probable in nature.

[1] J. C. Kemp, J. B. Swedlund, J. D. Landstreet, and J. R. P. Angel, Astrophys. J. **161**, L77 (1970).
[2] A. Putney, Astrophys. J. Lett. **451**, L67 (1995).
[3] G. D. Schmidt and P. S. Smith, Astrophys. J. **448**, 305 (1995).
[4] D. Reimers, S. Jordan, D. Koester, N. Bade, T. Koehler, and L. Wisotzki, Astron. Astrophys. **311**, 572 (1996).
[5] S. Jordan, in *White Dwarfs, Proceedings of the 10th European Workshop on White Dwarfs, held in Blanes, Spain, 17–21 June 1996*, edited by J. Isern, M. Hernanz, and E. Garcia-Berro, Astrophysics and Space Science Library Vol. 214 (Kluwer Academic Publishers, Dordrecht, 1997), p. 397.
[6] J. Nordhaus, S. Wellons, D. S. Spiegel, B. D. Metzger, and E. G. Blackman, Proc. Natl. Acad. Sci. U.S.A. **108**, 3135 (2011).
[7] S. Jordan, Astron. Astrophys. **265**, 570 (1992).
[8] J. R. P Angel, Annu. Rev. Astron. Astrophys. **16**, 487 (1978).
[9] G. Chanmugam, Annu. Rev. Astron. Astrophys. **30**, 143 (1992).
[10] D. Lai and S. L. Shapiro, Astrophys. J. **383**, 745 (1991).
[11] J. P. Ostriker and F. D. A. Hartwick, Astrophys. J. **153**, 797 (1968).
[12] V. L. Ginzburg, Sov. Phys. Dokl. **9**, 329 (1964).
[13] L. Woltjer, Astrophys. J. **140**, 1309 (1964).
[14] L. Spitzer, *Physical Processes in the Interstellar Medium* (Wiley, New York, 1978).
[15] S. L. Shapiro and S. A. Teukolsky, *Black Holes, White Dwarfs and Neutron Stars: The Physics of Compact Objects* (John Wiley and Sons, New York, 1983).
[16] S. Chandrasekhar, Mon. Not. R. Astron. Soc. **95**, 207 (1935).
[17] I.-S. Suh and G. J. Mathews, Astrophys. J. **530**, 949 (2000).

[18] A. Kundu and B. Mukhopadhyay, Mod. Phys. Lett. A **27**, 1250084-1 (2012).
[19] U. Das and B. Mukhopadhyay, Int. J. Mod. Phys. D **21**, 1242001 (2012).
[20] D. A. Howell *et al.*, Nature (London) **443**, 308 (2006).
[21] R. A. Scalzo *et al.*, Astrophys. J. **713**, 1073 (2010).
[22] I. Hachisu, M. Kato, H. Saio, and H. Nomoto, Astrophys. J. **744**, 69 (2012).
[23] L. D. Landau and E. M. Lifshitz, *Quantum Mechanics* (Pergamon, New York, 1977), 3rd ed..
[24] A. R. Choudhuri, *Astrophysics for Physicists* (Cambridge University Press, Cambridge, UK, 2010).
[25] A. M. Abrahams and S. L. Shapiro, Astrophys. J. **374**, 652 (1991).
[26] M. Sinha and B. Mukhopadhyay, arXiv:1005.4995.
[27] E. J. Ferrer, V. de La Incera, J. P. Keith, I. Portillo and P. L. Springsteen, Phys. Rev. C **82**, 5802 (2010).
[28] V. Dexheimer, R. Negreiros, and S. Schramm, arXiv:1108.4479.
[29] G. Chanmugam and M. Gabriel, Astron. Astrophys. **16**, 149 (1972).
[30] G. Fontaine, J. H. Thomas, and H. M. van Horn, Astrophys. J. **184**, 911 (1973).
[31] C. E. Wendell, H. M. van Horn, and D. Sargent, Astrophys. J. **313**, 284 (1987).
[32] A. Cumming, in *Magnetic Cataclysmic Variables, IAU Colloquium 190, Proceedings of the Conference Held 8–13 December 2002 in Cape Town, South Africa*, edited by S. Vrielmann and M. Cropper, ASP Conference Proceedings Vol. 315 (Astronomical Society of the Pacific, San Francisco, 2004), p. 58.
[33] J. S. Heyl and S. R. Kulkarni, Astrophys. J. Lett. **506**, L61 (1998).
[34] D. Bhattacharya, *Pulsar Timing, General Relativity and the Internal Structure of Neutron Stars*, edited by Z. Arzoumanian, F. Van der Hooft, and E. P. J. van den Heuvel (Koninklijke Nederlandse Akademie van Wetenschappen, Amsterdam, 1999).
[35] V. L. Ginzburg, J. Stat. Phys. **1**, 3 (1969).
[36] E. Østgaard, Z. Phys. **243**, 79 (1971).
[37] S. Konar and D. Bhattacharya, Mon. Not. R. Astron. Soc. **284**, 311 (1997).
[38] H. Y. Chiu and V. Canuto, Astrophys. J. **153**, L157 (1968).
[39] H. Y. Chiu, V. Canuto, and L. F. Canuto, Phys. Rev. **176**, 1438 (1968).
[40] V. Canuto and H. Y. Chiu, Space Sci. Rev. **12**, 3 (1971).
[41] J. K. Daugherty and I. Lerche, Phys. Rev. D **14**, 340 (1976).
[42] P. B. Jones, Mon. Not. R. Astron. Soc. **409**, 1719 (2010).
[43] D. Bandyopadhyay, S. Chakrabarty, and S. Pal, Phys. Rev. Lett. **79**, 2176 (1997).
[44] V. R. Khalilov, Phys. Rev. D **65**, 056001 (2002).
[45] L. Paulucci, E. J. Ferrer, V. de la Incera, and J. E. Horvath, Phys. Rev. D **83**, 043009 (2011).
[46] M. Bocquet, S. Bonazzola, E. Gourgoulhon, and J. Novak, Astron. Astrophys. **301**, 757 (1995).
[47] S. Bonazzola, E. Gourgoulhon, M. Salgado, and J. A. Marck, Astron. Astrophys. **278**, 421 (1993).